Geosci. Model Dev. Discuss., 7, 593–629, 2014
www.geosci-model-dev-discuss.net/7/593/2014/
doi:10.5194/gmdd-7-593-2014

Geoscientific Model Development Discussions
Open Access

A simple parameterization of the short-wave aerosol optical properties for surface direct and diffuse irradiances assessment in a numerical weather model

J. A. Ruiz-Arias[1,2,3] **and J. Dudhia**[3]

[1]Solar Radiation and Atmosphere Modeling Group, Physics Department, University of Jaén, Jaén, Spain
[2]Center of Advanced Studies in Energy and Environment, University of Jaén, Jaén, Spain
[3]Mesoscale and Microscale Meteorology Division, National Center for Atmospheric Research, Boulder, Colorado, USA

Received: 12 December 2013 – Accepted: 7 January 2014 – Published: 17 January 2014

Correspondence to: J. A. Ruiz-Arias (jararias@ujaen.es)

Published by Copernicus Publications on behalf of the European Geosciences Union.

Abstract

Broadband short-wave (SW) surface direct and diffuse irradiances are not typically within the set of output variables produced by numerical weather prediction (NWP) models. However, they are being more and more demanded in solar energy applications. A detailed representation of the aerosol optical properties is important to achieve an accurate assessment of these direct and diffuse irradiances. Nonetheless, NWP models typically oversimplify its representation or even neglect its effect. In this work, a flexible method to account for the SW aerosol optical properties in the computation of broadband SW surface direct and diffuse irradiances is presented. It only requires aerosol optical depth at 0.55 µm and the type of predominant aerosol. The rest of parameters needed to consider spectral aerosol extinction, namely, Angström exponent, aerosol single-scattering albedo and aerosol asymmetry factor, are parameterized. The parameterization has been tested in the RRTMG SW scheme of the Weather Research and Forecasting (WRF) NWP model. However, it can be adapted to any other SW radiative transfer band model. It has been verified against a control experiment along five radiometric stations in the contiguous US. The control experiment consisted of a clear-sky evaluation of the RRTMG solar radiation estimates obtained in WRF when RRTMG is driven with ground-observed aerosol optical properties. Overall, the verification has shown very satisfactory results for both broadband SW surface direct and diffuse irradiances. It has proven effective to significantly reduce the prediction error and constraint the seasonal bias in clear-sky conditions to within the typical observational error in well-maintained radiometers.

1 Introduction

Broadband SW surface total solar irradiance (also known as global horizontal irradiance, GHI) is the sum of broadband SW surface downward direct normal irradiance (DNI, received from the sun's direction) projected onto a horizontal plane and

GMDD
7, 593–629, 2014

broadband SW surface downward diffuse irradiance (DIF, received from other directions). In general, DIF may also include reflected irradiance from surrounding areas. Direct and diffuse components of GHI are rarely included in predictions made with Numerical Weather Prediction (NWP) models. As GHI is a key component in the representation of energy closure and mass surface fluxes, a better understanding and representation of physical processes may be gained through the use of DNI and DIF fluxes.

In the surroundings of gentle terrain, and provided the atmospheric state is known, GHI can be calculated at reasonable accuracy using simple models that assume isotropic sky and surface conditions. However, in cloudy skies or steep terrain, the isotropy assumption fails. In such a case, a 3-D solar radiation model would provide the best GHI predictions (Cahalan et al., 2005; Iwabuchi, 2006; Pincus and Evans, 2009). Nonetheless, these models are so computationally expensive that, in practice, their use is restricted only to concrete applications such as validation studies (Mayer et al., 2010) or the development of simplified parameterizations (Lee et al., 2011). But, if in particular both DNI and DIF are known, the uneven distribution of GHI over complex terrain areas can be determined. Projection of direct irradiance on tilted surfaces is a geometrical problem. The exact computation of diffuse irradiance over the surface would still be unfeasible but, in practice, isotropic or quasi-isotropic assumptions can be used at reasonable accuracy (Ruiz-Arias et al., 2010, 2011; Manners et al., 2012).

A better modelling of surface irradiance and its components is being also demanded by energy applications. Both GHI and DNI are acquiring greater importance in the energy sector as the rate of built-in solar systems is growing. On the one hand, traditional flat-photovoltaic (PV) systems, the more mature and widely-spread solar energy technology, are driven primarily by the incoming global irradiance onto the PV plane. As this plane very rarely coincides with the horizontal plane (the common irradiance output in most of the NWP models), a transposition model from the horizontal to the PV plane is inevitable; and accurate transposition models need DNI and DIF irradiances. On the other hand, solar concentrating technologies, both concentrating photovoltaic

GMDD
7, 593–629, 2014

and solar-thermal plants, are driven primarily by DNI. These technologies increase the overall efficiency of the systems by concentrating DNI using an optical assemble of mirrors. Overall, solar energy systems require long-term series of GHI and DNI fluxes over wide areas for a proper evaluation of the solar potential. But also, very importantly, they require forecasts that enable an improved operation of the plants and maximize the integration rate of solar systems in the power grid without putting in risk the power supply. This is best done with NWP models for most part of the forecasting time horizons (Diagne et al., 2013; Inman et al., 2013).

As it has been already brought up, among the set of radiative variables that can be predicted at surface, most of the NWP models only provide GHI. This has been very likely motivated by the fact that computation of DNI and DIF is challenging. But, at the same time, also because surface processes affected by solar radiation can be reasonably well represented with GHI alone, as long as spatial resolution stays above few km, which has been the typical case so far. Accurate calculation of DIF fluxes is computationally expensive compared with the simple methods that can be used to obtain GHI (Dudhia, 1989). Also, DNI and DIF are very sensitive, particularly DNI, to changes in the optically active components of the atmosphere. But the computational capabilities have grown enough to allow the use of more rigorous and precise methods to solve the atmospheric radiative transfer equation. Ruiz-Arias et al. (2013c) provide a comprehensive benchmarking study of some of the short-wave radiation schemes available in the Weather Research and Forecasting (WRF) NWP model at predicting GHI, DNI and DIF under clear-sky conditions in the contiguous US region. Albeit the evaluated models yielded GHI estimates within the observational error range, not all the modelling approaches showed good skills at predicting DNI and DIF. The best results were achieved with the Rapid Radiative Transfer Model for climate and weather models (RRTMG; Iacono et al., 2008). In particular, for the period evaluated, the mean and root-mean square DNI errors when the RRTMG model was run without considering aerosol extinction (default setting in WRF) were 66 $W m^{-2}$ (7 %) and 72 $W m^{-2}$ (8 %), respectively (percent magnitudes are relative to the mean observed value). In contrast,

GMDD
7, 593–629, 2014

when RRTMG was run with instantaneous observations of aerosol optical properties (hereinafter, AOP), the mean and root-mean square errors diminished to 0 $W m^{-2}$ (0 %) and 9 $W m^{-2}$ (1 %), respectively. In the case of DIF, the mean and root-mean square errors when the model was not driven by AOP observations were −26 $W m^{-2}$ (−34 %) and 28 $W m^{-2}$ (37 %), respectively. When AOP observations were used, the mean and root-mean square errors decreased to 2 $W m^{-2}$ (3 %) and 5 $W m^{-2}$ (6 %), respectively.

2 The need for a AOP parameterization

Nowadays many of the NWP models solve, or may solve, the solar radiative transfer in the atmosphere using a two-stream approach, which allows for a fast and approximated solution by assuming azimuthal isotropy in radiant fluxes (Ritter and Geleyn, 1992; Edwards and Slingo, 1996; Chou et al., 1998; Iacono et al., 2008). Radiative transfer solvers in NWP models have been tailored by assuming an infinite and horizontally uniform atmosphere and treating each model column independently. The major practical consequence of the two-stream approximation is an accuracy diminishing for large solar zenith angles. However, it is accurate enough at other conditions for most of the current applications. It allows for a sufficiently detailed description of the solar direct and diffuse fluxes at a low-to-moderate spectral resolution.

In the absence of clouds, aerosols become the dominant driving factor for DNI and DIF fluxes and the greatest source of uncertainty. In particular, the impact of aerosols in DNI is about 3 to 4 times larger than it is in GHI (Gueymard, 2012; Ruiz-Arias et al., 2013a) since an increase (decrease) of aerosol extinction results in a decrease (increase) of DNI and an increase (decrease) of DIF, in the general case. Thus, errors in DNI and DIF fluxes caused by a misrepresentation of the aerosol load cancel out in GHI. In part, this explains why many NWP models have traditionally neglected the direct impact of aerosol in the assessment of GHI, or why it has been simply accounted for by using climatological values. However, this may result in DNI assessment errors up to 20 % (Ruiz-Arias et al., 2013a, c).

GMDD
7, 593–629, 2014

Extinction by aerosols is described in radiative transfer problems in terms of three spectral quantities, namely, aerosol optical depth (AOD or τ), single-scattering albedo (SSA or ω_0) and asymmetry factor (ASY or g). Aerosol optical depth is the integral of the extinction coefficient over a vertical path. It represents the attenuation of radiation by absorption and scattering events over the vertical path. Single-scattering albedo is the ratio of the scattering and extinction efficiencies. It represents the relative importance of the scattering events within the total extinction. Finally, asymmetry factor is the first moment of the scattering phase function. It accounts for the preferred direction in which radiation is scattered (Liou, 2002). It is usual to model the spectral variability of AOD using the Ångström law $\tau(\lambda) = \beta\lambda^{-\alpha}$, where λ is the wavelength in µm, β is the AOD measured at $\lambda = 1$ µm and α is known as Ångström exponent (AE) (Ångström, 1961).

The number and variety of region-wide aerosol datasets has steadily grown in the recent years, from worldwide ground datasets as the Aerosol Robotic Network (AERONET; Holben et al., 1998) to sensors aboard satellite platforms that regularly surround the globe, being the Moderate resolution Imaging Spectro-radiometer (Remer et al., 2005) the best well-known. Both provide AOP observations that could be used in NWP models to compute DNI and DIF fluxes. Ground observations, essentially from AERONET, provide a reliable and comprehensive AOP description, at a number of wavelengths. However, the spatial coverage is scarce and its near-real-time availability is limited. Thus, in practice, its applicability to NWP model applications is constrained to a reduced number of cases. Satellite retrievals, on the opposite, provide broad spatial coverage but the accuracy of their current estimates is often only reasonable for AOD at 0.55 µm. Also in recent years, and leveraged by the growing number of available ground and remote sensing datasets, the coupled Atmosphere–Chemistry Numerical Weather Prediction (ACNWP) models have experienced a big advance and now they routinely offer global forecasts of many molecular and particulate components of the atmosphere. Such is the case of the Monitoring Atmospheric Composition and Climate project (MACC, 2013) or the Goddard Earth Observing System model version 5

GMDD
7, 593–629, 2014

(GEOS-5, 2013). They compute AOP from prognoses of the chemical composition of the atmosphere and use them to calculate DNI and DIF fluxes. Nonetheless, in general, ACNWP models are computationally expensive and complex to run compared with the regular limited-area NWP models. Also, as they are initialized using mostly satellite observations, they suffer of similar biases regarding optical properties of aerosols.

For those applications that are focused on DNI and DIF fluxes, it is convenient to set up a means to use AOP inputs in NWP models from different sources. This approach would allow using the best aerosol optical source for each application. In particular, for long-term evaluations of the regional surface solar radiation potential, combined measurements of satellite and ground sites could be used (Ruiz-Arias et al., 2013b). On the other hand, when the application requires forecasts of surface solar radiation, the AOP predicted by global ACNWP models could be used. Nonetheless, as the only accurate aerosol optical parameter typically available is AOD, the rest of required parameters, namely, SSA, ASY and AE, need to be specified/parameterized based on additional information.

In this work, a parameterization approach for the aerosol optical parameters required by radiative transfer models other than AOD at 0.55 µm is described. In particular, SSA, ASY, and AE are parameterized as a function of built-in reference aerosols and relative humidity. The method is verified in the WRF NWP model using the RRTMG short-wave radiative scheme against a previous experiment in which RRTMG was driven with observed AOD at 0.55 µm, SSA, ASY, AE and precipitable water gathered in the AERONET network. This control experiment is thoroughly described in Ruiz-Arias et al. (2013c). Afterwards, the benefits of the AOP parameterization were evaluated based on the comparison of 1 yr WRF simulation against independent surface solar irradiance ground observations in the contiguous US.

Section 3 describes the approach taken for the parameterization of the aerosol optical properties in the RRTMG short-wave radiative transfer model. Sections 4 and 5 present the results of a benchmarking study against a control experiment and the

GMDD
7, 593–629, 2014

validation against ground observations, respectively. Finally, Sect. 6 highlights the most important conclusions of this work.

3 The AOP parameterization

The RRTMG SW radiative transfer model solves multiple scattering using a two-stream algorithm (Oreopoulos and Barker, 1999) over 14 spectral bands spanning from 0.2 to 12.2 µm (Table 1). It accounts for extinction by water vapor, carbon dioxide, ozone, methane, oxygen, nitrogen, aerosols, Rayleigh scattering and clouds. In clear skies, the expected accuracy of RRTMG with respect to line-by-line calculations is about 4 $W m^{-2}$ for direct fluxes and about 5 $W m^{-2}$ for diffuse fluxes (Iacono et al., 2008).

Aerosol optical properties, that must be provided to the radiative transfer routine at every grid-cell of the simulating domain and each spectral band, have been parameterized in terms of the vertically-integrated (total) AOD at 0.55 µm ($\tau_{0.55}$) and built-in reference aerosols. The reason is twofold: on the one hand, optical depth is the most determinant property in the solar extinction burden, so it is important to make use of the best estimate available. On the other hand, unlike other aerosol optical properties, both satellite retrievals and ACNWP models provide reasonable estimates of AOD for many current applications. The reason to choose the value at 0.55 µm is to be consistent with the values usually provided by these data sources and the ground observations at AERONET. The latter can be easily interpolated to a wavelength of 0.55 µm from other spectral values by using the Ångström law. The reference aerosol type is used to provide spectral climatic values for SSA, ASY and AE, which are afterwards modulated in terms of the relative humidity to account for the aerosol hygroscopicity.

Two different reference aerosols from Shettle and Fenn (1979), namely rural and urban, representative of broad inland conditions have been included so far in WRF. The rural aerosol is intended for situations where the aerosol is not expected to be affected by urban or industrial sources. It will be thus the typical choice for most of the simulations. It is composed of a mixture of 70 % of water soluble substance and 30 % dust-like

GMDD
7, 593–629, 2014

aerosols. The urban aerosol is a mixture of rural aerosol (80 %) and soot-like particles (20 %). The two reference types define the absorption, scattering and extinction coefficients, single-scattering albedo and asymmetry parameter for a number of wavelengths and relative humidities from 0 % to 99 %. The choice of these two reference aerosols was based on the fact that they are two well known models. Experience gained with its use may be used to incorporate more specific aerosol types.

3.1 Aerosol optical depth and Ångström exponent

Aerosol optical depth has to be specified at each model spectral band. In real applications, even in the best cases, AOD is only known/measured at a small number of wavelengths, and the Ångström law is often used to describe its spectral variability. But, for some aerosol particle ensembles, such as the reference aerosol types used here, this spectral variability is best described using a 2-band version of the Ångström law (Gueymard, 2001) as follows:

$$\tau(\lambda) = \tau_{0.55} \left(\frac{\lambda}{0.55} \right)^{-\alpha_i}, \quad (1)$$

where λ is the wavelength in μm and α_i is the Ångström exponent for each band, defined as $\alpha_i = \alpha_1$, for $\lambda < 0.55$ μm, and $\alpha_i = \alpha_2$, otherwise. The coefficients α_i are obtained from the built-in reference aerosol types by linearly fitting (in log-log coordinates) the spectral extinction coefficients tabulated in Shettle and Fenn (1979) for each aerosol type and relative humidity. The corresponding values of α_i are given in Table 2. For α_1, the extinction coefficients at 0.337 μm, 0.55 μm and 0.649 μm were used. The values at 0.649 μm, 1.06 μm and 1.536 μm were used for α_2. Note that the very different values obtained for α_1 and α_2 indicate that the 2-band Ångström model is more appropriate than the original one. The decreasing α_i values for high relative humidities indicate a particle size increase and a shift of the extinction towards lower wavelengths.

The spectral AOD was averaged over each spectral band in order to provide a representative value over the entire band. As the solar spectral irradiance changes abruptly

GMDD
7, 593–629, 2014

in the ultraviolet and visible regions and some model bands in the infrared region are wide, the extraterrestrial solar spectrum, $E_{0n}(\lambda)$, as described by Gueymard (2004), was used as weighting factor to compute the average AOD value, $\bar{\tau}_{rj}$, as follows:

$$\bar{\tau}_{rj} = \frac{\int_{\Delta\lambda_j} E_{0n}(\lambda_j)\tau_r(\alpha_{ri};\lambda_j)\mathrm{d}\lambda_j}{\int_{\Delta\lambda_j} E_{0n}(\lambda_j)\mathrm{d}\lambda_j}, \quad (2)$$

where j stands for each RRTMG spectral band, that extends over the range $\Delta\lambda_j$, and $\tau_r(\alpha_{ri};\lambda_j)$ is the aerosol optical depth calculated with Eq. (1) for the relative humidity r. Factorizing $\tau_{0.55}$ out of $\tau_r(\alpha_{ri};\lambda_j)$, Eq. (2) can be re-written as

$$\bar{\tau}_{rj} = \rho_{rj}\tau_{0.55} \quad (3)$$

where ρ_{rj} is the spectral scale factor with respect to $\tau_{0.55}$ for the band j and relative humidity r. It is given by

$$\rho_{rj} = \frac{\int_{\Delta\lambda_j} E_{0n}(\lambda_j)\left(\frac{\lambda_j}{0.55}\right)^{-\alpha_{ri}}\mathrm{d}\lambda_j}{\int_{\Delta\lambda_j} E_{0n}(\lambda_j)\mathrm{d}\lambda_j}. \quad (4)$$

Equation (4) was numerically evaluated for each spectral band and relative humidity according to the α_i coefficients in Table 2. The so-computed spectral scale factor values ρ_{rj} were grouped in two look-up-tables for the two aerosol types (Tables A1 and A2). For each model spectral band, the spectral scaling factors are interpolated using a 4-points Lagrange interpolation at the relative humidity values predicted by the NWP model. Aerosol optical depth is then calculated using Eq. (3) and the input $\tau_{0.55}$. Figure 1 exemplifies the interpolation results for the rural aerosol type. It also compares the weighted average as defined by Eq. (2) with a regular (un-weighted) average. The largest discrepancies appear in the ultraviolet, visible and near-infrared regions (bands 8–12) as well as in the mid-infrared region (band 14). The weighted average shifts the

GMDD
7, 593–629, 2014

averaged AOD value towards wavelengths with higher extraterrestrial solar intensity resulting in an enhancement of aerosol extinction in the visible and infrared bands, and a decreased extinction in the ultraviolet region.

3.2 Single-scattering albedo and asymmetry factor

Shettle and Fenn (1979) provide spectral values of SSA and ASY up to 40 µm starting at 0.2 µm for each aerosol type and relative humidity value. Single-scattering albedo has been spectrally weighted for each band as follows:

$$\bar{\omega}_{o,rj} = \frac{\int_{\Delta\lambda_j} E_{on}(\lambda_j)\hat{\omega}_{o,r}(\lambda_j)\tau_r(\alpha_{ri};\lambda_j)\mathrm{d}\lambda_j}{\int_{\Delta\lambda_j} \tau_r(\alpha_{ri};\lambda_j)E_{on}(\lambda_j)\mathrm{d}\lambda_j}, \quad (5)$$

where $\bar{\omega}_{o,rj}$ is the average SSA value for the relative humidity r and the spectral band j. The tabulated values of SSA for each relative humidity were interpolated using cubic splines to the wavelengths at which $E_{on}(\lambda_j)$ is known, resulting in the values $\hat{\omega}_{o,r}(\lambda_j)$. Equation (5) assigns a higher weight to the wavelengths at which extraterrestrial solar spectral irradiance and aerosol extinction are greater. The values $\bar{\omega}_{o,rj}$ were grouped in two look-up-tables for the two aerosol types (Tables A3 and A4) from which values are interpolated for each spectral band and relative humidity using a 4-points Lagrange interpolation.

Following a similar approach, spectrally-averaged asymmetry factor has been calculated as:

$$\bar{g}_{rj} = \frac{\int_{\Delta\lambda_j} E_{on}(\lambda_j)\hat{g}_r(\lambda_j)\hat{\omega}_{o,r}(\lambda_j)\tau_r(\alpha_{ri};\lambda_j)\mathrm{d}\lambda_j}{\int_{\Delta\lambda_j} \hat{\omega}_{o,r}(\lambda_j)\tau_r(\alpha_{ri};\lambda_j)E_{on}(\lambda_j)\mathrm{d}\lambda_j}, \quad (6)$$

where $\bar{g}_{rj}$ is the average ASY value for the relative humidity r and the spectral band j. The tabulated values of ASY for each relative humidity were interpolated using cubic splines to the wavelengths at which $E_{on}(\lambda_j)$ is known, resulting in the values $\hat{g}_r(\lambda_j)$.

GMDD
7, 593–629, 2014

In this case, a higher weight has been assigned at those wavelengths with greater $E_{on}(\lambda_j)$ and scattering coefficient. The values $\bar{g}_{rj}$ were grouped in two look-up-tables for the two aerosol types (Tables A5 and A6) from which values are interpolated for each spectral band and relative humidity using a 4-points Lagrange interpolation.

Figure 2 shows the parameterized SSA and ASY values for the two built-in reference aerosols for a relative humidity of 80 %. The solid thin line is the resulting interpolation from the tabulated values (cross marks) in Shettle and Fenn (1979), both for SSA and ASY. The solid thick line is the resultant weighted average for each model band after applying Eqs. (5) and (6). The shaded region represents the range of variability at each band due to relative humidity, from 0 % to 99 %. In general, SSA for the urban aerosol (Fig. 2c) has a smaller value at all wavelengths and a higher sensitiviy to relative humidity changes than the rural type (Fig. 2a). Thus, the latter scatters more radiation but responds less to changes in humidity. Note that, for wavelengths above 4 µm, the band-averaged SSA keeps close to the SSA value between 4 and 5 µm because the extraterrestrial solar intensity is very small beyond 5 µm. Asymmetry factor is very similar for the two reference aerosol types (Fig. 2b and d), with decreasing forward scattering in the ultraviolet and visible bands and increasing in the infrared up to 3 µm. Beyond, it stays at about 0.75.

3.3 Vertical distribution

The vertical distribution of AOD is modelled after the spectral disaggregation has been completed. The latter is made following Eq. (3) with spectral scale values ρ_{rj} interpolated according to the model relative humidity, but only at surface level. Then, the spectrally disaggregated $\bar{\tau}_j$ values at surface for each band are distributed in the vertical according to an exponential profile (Ruiz-Arias et al., 2013c) as follows:

$$\bar{\tau}_j(z) = \frac{\bar{\tau}_j / Z_\mathrm{h}}{e^{-\frac{z_\mathrm{sfc}}{Z_\mathrm{h}}} - e^{-\frac{z_\mathrm{toa}}{Z_\mathrm{h}}}} \int_z^{z_\mathrm{toa}} e^{-\frac{z}{Z_\mathrm{h}}} \mathrm{d}z, \tag{7}$$

GMDD
7, 593–629, 2014

where z_{sfc} and z_{toa} are the altitudes at surface and the top of the atmosphere, respectively. The height scale parameter Z_h is set to 2.5 km (Gueymard and Thevenard, 2009). By following this procedure the vertically-integrated profile of AOD is consistent with the $\tau_{0.55}$ value provided as input.

The vertical distribution of SSA and ASY is based only on the relative humidity profile in the NWP model. Therefore, the SSA and ASY vertical profiles resemble the model moisture profile.

4 Parameterization benchmarking

The consistency of the AOP parameterization at predicting clear-sky surface solar irradiance has been first benchmarked against a case study (hereinafter referred to as control experiment) in which the WRF's RRTMG model was driven with observed aerosol optical properties and precipitable water in a number of sites of the AERONET network with collocated surface solar irradiance observations. The control experiment represents a best-case estimate of the expected model performance at predicting clear-sky surface solar irradiance.

4.1 Control experiment

In the control experiment, the WRF model was run using the RRTMG SW scheme. Clear-sky estimates of GHI, DNI and DIF were computed every 10 min for five completely cloudless days at five different locations in the contiguous US (see Ruiz-Arias et al., 2013c, for a description of the sites). At all sites, concurrent observations of GHI, DNI and DIF, as well as aerosol optical properties and precipitable water from nearby AERONET locations, were available. Four of the experimental surface solar irradiance sites belong to the Baseline Surface Radiation Network (BSRN; Ohmura et al., 1998) and the Surface Radiation Network (SURFRAD; Augustine et al., 2005). The fifth is at the Atmospheric Radiation Measurement (ARM, 2013) Central Facility, OK. The WRF

GMDD
7, 593–629, 2014

model was modified such that instantaneous observations of all the aerosol optical properties and precipitable water could be ingested every 10 min at exactly the same time steps at which solar irradiance was computed. The few traces of clouds generated by WRF during the simulations were cleared up to ensure results under completely clear-sky conditions. Note that, as all the aerosol optical properties were ingested from ground observations, there was no need to parameterize any aerosol property. The control experiment is fully described in Ruiz-Arias et al. (2013c).

4.2 Test case

The simulations of the control experiment were repeated using the AOP parameterization. That is, only the observed AOD at 0.55 µm at the AERONET sites and the type of aerosol were provided to WRF. The rest of aerosol parameters, namely, AE, SSA and ASY, were parameterized, as presented in Sect. 3. As in the control experiment, the model was driven with observations of precipitable water so that the real skill of the aerosol parameterization was better evaluated. Two different simulations, assuming rural and urban aerosol types, were carried out at each site. An additional one, without aerosol inputs was also conducted.

Figure 3 shows the relative errors of both the control experiment and the test cases as compared against the GHI, DNI and DIF ground observations at each site and the composite of all sites. If the parameterization were perfect, the grey blocks and the colour bars should match. Disagreements are caused by the prescription of the aerosol type.

Figure 3a shows the relative errors in the case of DNI. As it was expected, the discrepancies between the control experiment and the test cases using the AOP parameterization are negligible (below 1 % at all sites), regardless the aerosol type. The reason is that, as far as aerosols concern, DNI is only impacted by optical depth, and the AOD at 0.55 µm is the same in both the control experiment and the test cases. The only distinction between the experiments is the AOD spectral distribution, modelled by the AE value. In the control experiment, it comes from spectral observations of AOD. However,

GMDD
7, 593–629, 2014

in the test cases, it is inferred from the selected aerosol type and the relative humidity. Nonetheless, as DNI is a broadband quantity, the impact of AE is small and so are the differences between the control experiment and the test cases. On the contrary, when no aerosols are used, the simulated DNI overestimates the observations beyond the expected observational error.

Figure 3b shows the relative errors in the case of DIF. Now, discrepancies between the control experiment and the test cases are greater because DIF is also impacted by SSA and ASY, which now are parameterized. Specifically, for relative humidities below 90 %, the parameterized SSA spectral values for the rural aerosol type are about 20 % to 40 % greater than in the case of the urban aerosol type. As a consequence, systematic disagreements up to 15–20 % appear in the DIF values computed with the two aerosol types. Hence, unlike for the DNI, the choice of the correct aerosol type is important for DIF. In particular, at four of the sites evaluated in this study, the rural aerosol type fits reasonably well the control experiment. On the contrary, at the TBL site the urban aerosol yielded better results because the particular selection of clear-sky days at this site showed anomalously low SSA values (Ruiz-Arias et al., 2013c), more representative of an urban aerosol type. These values could be explained by a forest fire nearby so they do not necessarily mean that the typical type of aerosol at the TBL site is urban. When the model is not driven by aerosols, a systematic underestimation around 30 % appears.

In the case of GHI (Fig. 3c), all the experiments provide estimates within the expected observational error range, even when aerosols are not provided because the large overestimation in DNI is cancelled out with the large underestimation in DIF. Overall, the rural aerosol type fits better the control experiment.

5 Validation against ground observations

A major limitation of the benchmarking study described in the former section comes from the fact that AOD, AE, SSA and ASY need to be known simultaneously in the

GMDD
7, 593–629, 2014

control experiment. Measurement of SSA and ASY is limited by strong practical constraints (Dubovik et al., 2000) that reduce drastically their availability. Nonetheless, as the only external input required by the AOP parameterization is AOD at 0.55 µm, the validation period with the AOP parameterization can be extended as long as AOD and surface solar irradiance measurements are available. Thereby, two one-year-length simulations have been conducted using the AOP parameterization with rural and urban aerosols at the same five sites described in Sect. 4 and with the same model set-up. In particular, the AOD at 0.55 µm from the AERONET sites was ingested into WRF every 10 min at exactly the same time steps at which GHI, DNI and DIF were computed. The subsequent validation was conducted only for those time steps with AOD observations under clear-sky conditions, which were discerned based on the method described in Long and Ackerman (2000).

In addition, the simulation was repeated using the WRF's Dudhia SW scheme as a skill reference for the case of GHI. The Dudhia SW scheme is the broadband radiative transfer model of choice in most of the WRF runs. It only provides estimates for GHI.

5.1 Dynamical range performance

The performance of the AOP parameterization for each aerosol type has been analysed throughout the entire range of variability of the aerosol optical properties observed in this experiment for the composite of the five experimental sites. Figure 4a–c shows the relative frequency distribution of the observed AOD at 0.55 µm, the observed and parameterized SSA values, and the observed and parameterized ASY values, respectively. Overall, the AOD values in the validation sites are small, although the evaluation period spans an entire year and includes all the available observations in the sites. The mean value is 0.06, the median is at 0.05 and 95 % of the values are smaller than 0.12. The mean observed SSA value is 0.92 (Fig. 4b), with 95 % of the values greater than 0.75. A very distinct estimation of the SSA values is made with the rural and urban types. Whereas 95 % of the rural SSA values are between 0.4 and 0.92, with its mean value in 0.93, the urban SSA values are far from the observed ones. In particular, 95 %

GMDD
7, 593–629, 2014

of the values are smaller than 0.68, and the mean value is 0.62. Figure 4c shows the relative frequency distribution of observed and simulated ASY values. A 95 % of the observations span the range from 0.61 to 0.75, with a mean value of 0.67. The values simulated by the rural aerosol have the mean in 0.66, and 90 % of the data spans from 0.63 to 0.67. In the case of the urban aerosol, 90 % of the aerosols span from 0.66 to less than 0.67, and the mean is also in 0.66.

As AE is not directly parameterized (note that it has been approximated by means of a two-band model), it has not been shown for the sake of simplicity. However, its effective value can be estimated from the spectral distribution of AOD throughout the RRTMG bands. When that is done, 99 % of the AE values for the rural aerosol are between 1.19 and 1.22, and 99 % of the AE values for the urban aerosol are in the range from 1.00 to 1.06. In contrast, 90 % of the observations go from 0.72 up to 2.59. Note thus that, the effective AE values used in the parameterization do not span the range of observed AE values.

Figure 4d–f shows the results for DNI. In any case, the relative error is within the expected DNI observational error. However, as it can be seen in Fig. 4d, for AOD above 0.05, there is a systematic bias of about 4 Wm^{-2} between the estimates with the rural and urban aerosol types. A experiment (not shown here for the sake of conciseness) conducted with the SMARTS radiative transfer model (Gueymard, 2001) has revealed this discrepancy is compatible with the different AE values modelled by each aerosol type. For AOD values below 0.05, the disagreement with the observations increases slightly. As it is shown in Ruiz-Arias et al. (2013c), this might be related to the observational uncertainty of the AOD observations taken at AERONET sites. As it is expected, DNI does not show any apparent trend with SSA and ASY (Fig. 4e and f).

Figure 4g–i shows the results for DIF. For these sites, and for all cases, the DIF estimates assuming the rural aerosol type are within the expected range of the observational error. However, the urban aerosol type shows a negative bias that, in particular, increases in magnitude for increasing AOD. The reason is that there exists a positive correlation between AOD and SSA in this experimental dataset (not shown here) such

GMDD
7, 593–629, 2014

as an increase of AOD entails an increase of SSA. In addition, as it is shown in Fig. 4h, there exists a systematic underestimation of about 15 % in the estimated DIF values assuming urban type aerosol, whereas it stays unbiased for the rural aerosol type. No trend is observed in the simulated DIF values with respect to ASY (Fig. 4i).

Figure 4j–l shows the results for GHI. Besides GHI computed with the RRTMG model assuming rural and urban aerosol types, GHI calculated with the Dudhia SW scheme is also shown. It does not make use of any aerosol optical variable as input. In any case, all the simulated values are within the range of the expected observational error. In particular, GHI estimates with the RRTMG model assuming rural aerosol are always unbiased. On the contrary, when the urban aerosol type is assumed, the bias in DIF (Fig. 4g–i) appears in GHI but with a reduced relative impact (about 3 %). The Dudhia scheme shows an increasing trend with respect to AOD at 0.55 µm that goes from about 5 % (or, equivalently, 25 $W m^{-2}$) for very clean conditions to unbiased estimates for AOD about 0.12, as expected for a scheme with a fixed aerosol scattering parameter. No trend is observed with respect to SSA and ASY.

5.2 Seasonality

One of the particular benefits of having a method to include aerosol extinction in the computation of surface solar irradiance is to consider the impact of the seasonal variability of AOD in surface fluxes. Specifically, if AOD is not considered in the calculation of clear-sky surface irradiance, or it is done using a fixed value, a seasonal bias may appear in the computed irradiances at surface, which can become considerably large depending on the simulated region. Figure 5 shows the daily mean relative error in computed DNI, DIF and GHI (simulated values minus observations) using the RRTMG model assuming rural and urban aerosol types, throughout the simulated year over the composite of the five experimental sites. A 15 day moving average filter has been used to make clear the bias trend. For GHI, the calculated values with the Dudhia scheme are also shown. The expected observational error region for the surface solar irradiance observations, roughly estimated as ±5 %, is highlighted in yellow.

GMDD
7, 593–629, 2014

Figure 5a and b shows the case of DNI and DIF estimates, respectively. Overall, both rural and urban aerosol types produce unbiased DNI values during the entire simulated year. The little disagreement between them is due to the different AE values that are parameterized by each aerosol type. Regarding DIF, the urban aerosol type yields a sustained bias around −15 %, with no seasonal trend, whereas the bias using the rural aerosol type stays within the expected observational error region, also without clear seasonal trend. Note that it proves the rural aerosol model fits the observations better for the evaluated sites.

Figure 5c shows the results for GHI. The values computed with the RRTMG model assuming the rural aerosol type are unbiased throughout the entire simulated year, whereas the assumption of urban aerosol type introduces a negative bias about −2 %. But no seasonal trend is observed in any of these two cases. On the contrary, the Dudhia model shows a clear seasonal trend in the bias, which underestimates up to a 5 % in winter, as it includes atmospheric scattering by a fixed empirical fit to GHI observations and considers the scattering in a yearly basis. It cannot reproduce its intra-annual variability.

6 Discussion and conclusions

A parameterization of the aerosol optical properties for short-wave surface solar irradiance assessment, including direct and diffuse components, in NWP models has been proposed. It has been implemented and verified in the RRTMG SW scheme of the WRF NWP model. The verification has been conducted among five radiometric stations with nearby or collocated AERONET sites in the contiguous US and relies on a previous experiment that has been used here as control case. The control experiment consisted on a best-case clear-sky evaluation of some of the WRF short-wave solar radiation schemes forced with observed aerosol optical properties taken at the AERONET sites. Thus no aerosol optical property is parameterized in the control experiment. On the contrary, the aerosol optical parameterization only uses observations

GMDD
7, 593–629, 2014

of AOD at 0.55 µm, and AE, SSA and ASY are parameterized based on the predominant type of aerosol and the relative humidity. Both rural and urban aerosol types have been tested.

The approach to parameterize the aerosol optical properties is versatile since the only mandatory parameter is AOD at 0.55 µm, that can be either provided as a fixed value or as a time and space varying field. The rest of aerosol optical parameters, namely, AE, SSA and ASY are parameterized from a choice among rural or urban aerosol types, as it has been described in the paper. However, as for AOD at 0.55 µm, they can also be either provided as a fixed value or as a time and space varying field. This allows for sensitivity studies or the use of external data sources. The aerosol parameterization based on the aerosol type choice allows us to extend the evaluation period up to one year, beyond the comparison with the control case. Overall, the verification has shown very satisfactory results. Regardless of the type of aerosol invoked, DNI using the AOP parameterization is almost identical to the control case. The very small mismatches result from the parameterization of AE. When the focus is on DIF, the selection of the right aerosol type is important because DIF is affected also by SSA and ASY. In four of the experimental sites, the rural aerosol type resulted in very good agreement with the control case. In the remaining site, the observed SSA in the AERONET station during the days simulated in the control experiment presented anomalously low values. This explains why the urban aerosol type is better there and proves that its use can be effective in sites with typical urban aerosols. Based on the 1 yr simulation, it has been proved that the use of the AOP parameterization to consider fluctuating aerosols contributes to effectively remove seasonal biases in DNI, DIF and GHI. In the latter case, this has been illustrated by comparing the results against the Dudhia short-wave scheme that considers aerosol extinction by assuming a single yearly value.

Arguably, the major limitation of the AOP parameterization might be the requirement to adhere to one of the prescribed type of aerosols; namely, rural and urban, in this particular case study. However, even this simple approach has proven very effective

GMDD
7, 593–629, 2014

in the evaluated sites and it can be presumed that it will be so in their surroundings. Thus, the approached method makes sense for limited-area models. Note also that the range of AOD values involved in the 1 yr runs is rather limited. However, these were the actual AOD values observed during one entire year at the experimental sites and it can be seen as representative of these locations. Notwithstanding, it is evident that they do not cover all the possible range of climatic situations regarding aerosols and new aerosol types should be incorporated and validated. Of particular interest for solar energy applications is the case of desert areas, dominated by dust aerosols, since they hold much of the worldwide solar energy potential.

Acknowledgements. The authors would like to thank the BSRN, NOAA, and AERONET science teams, and the ARM Climate Research Facility, for establishing and maintaining the sites used in this investigation. The authors also warmly thank Christian A. Gueymard for his unbounded support and stimulating discussions in the course of this research. José A. Ruiz-Arias is funded by a Marie Curie Action under the project PIOF-GA-2010-273648 within the 7th European Community Framework Programme, the Spanish Ministry of Science and Innovation under the project CGL2011-30377-C02-01 and FEDER funds through the Junta de Andalucia research group TEP-220. This work was carried out while the author was hosted by NCAR.

References

Ångström, A.: Techniques of determinig the turbidity of the atmosphere 1, Tellus, 13, 214–223, 1961. 598

ARM: available at: http://www.arm.gov/sites/sgp/c (last access: 7 November), 2013. 605

Augustine, J. A., Hodges, G. B., Cornwall, C. R., Michalsky, J. J., and Medina, C. I.: An update on SURFRAD – the GCOS Surface Radiation budget network for the continental United States, J. Atmos. Ocean. Tech., 22, 1460–1472, 2005. 605

Cahalan, R. F., Oreopoulos, L., Marshak, A., Evans, K. F., Davis, A. B., Pincus, R., Yetzer, K. H., Mayer, B., Davies, R., Ackerman, T. P., Barker, H. W., Clothiaux, E. E., Ellingson, R. G., Garay, M. J., Kassianov, E., Kinne, S., Macke, A., O'Hirok, W., Partain, P. T., Prigarin, S. M., Rublev, A. N., Stephens, G. L., Szczap, F., Takara, E. E., Várnai, T., Wen, G., and Zhuravleva,

GMDD
7, 593–629, 2014

T. B.: THE I3RC: bringing together the most advanced radiative transfer tools for cloudy atmospheres, B. Am. Meteorol. Soc., 86, 1275–1293, 2005. 595
Chou, M.-D., Suarez, M. J., Ho, C.-H., Yan, M. M., and Lee, K.-T.: Parameterizations for cloud overlapping and shortwave single-scattering properties for use in general circulation and cloud ensemble models, J. Climate, 11, 202–214, 1998. 597
Diagne, M., David, M., Lauret, P., Boland, J., and Schmutz, N.: Review of solar irradiance forecasting methods and a proposition for small-scale insular grids, Renew. Sust. Energ. Rev., 27, 65–76, 2013. 596
Dubovik, O., Smirnov, A., Holben, B., King, M., Kaufman, Y., Eck, T., and Slutsker, I.: Accuracy assessments of aerosol optical properties retrieved from Aerosol Robotic Network (AERONET) sun and sky radiance measurements, J. Geophys. Res.-Atmos., 105, 9791–9806, 2000. 608
Dudhia, J.: Numerical study of convection observed during the winter monsoon experiment using a mesoscale two-dimensional model, J. Atmos. Sci., 46, 3077–3107, 1989. 596
Edwards, J. and Slingo, A.: Studies with a flexible new radiation code. I: Choosing a configuration for a large-scale model, Q. J. Roy. Meteor. Soc., 122, 689–719, 1996. 597
GEOS-5: available at: http://gmao.gsfc.nasa.gov/GEOS/ (last access: 7 November), 2013. 599
Gueymard, C. A.: Parameterized transmittance model for direct beam and circumsolar spectral irradiance, Sol. Energy, 71, 325–346, 2001. 601, 609
Gueymard, C. A.: The Sun's total and spectral irradiance for solar energy applications and solar radiation models, Sol. Energy, 76, 423–453, 2004. 602
Gueymard, C. A.: Temporal variability in direct and global irradiance at various time scales as affected by aerosols, Sol. Energy, 86, 3544–3553, 2012. 597
Gueymard, C. A. and Thevenard, D.: Monthly average clear-sky broadband irradiance database for worldwide solar heat gain and building cooling load calculations, Sol. Energy, 83, 1998–2018, 2009. 605
Holben, B., Eck, T., Slutsker, I., Tanre, D., Buis, J., Setzer, A., Vermote, E., Reagan, J., Kaufman, Y., Nakajima, T., Lavenu, F., Jankowiak, I., and Smirnov, A.: AERONET: a federated instrument network and data archive for aerosol characterization, Remote Sens. Environ., 66, 1–16, 1998. 598
Iacono, M. J., Delamere, J. S., Mlawer, E. J., Shephard, M. W., Clough, S. A., and Collins, W. D.: Radiative forcing by long-lived greenhouse gases: calculations with the AER radiative trans-

GMDD
7, 593–629, 2014

fer models, J. Geophys. Res.-Atmos., 113, D13103, doi:10.1029/2008JD009944, 2008. 596, 597, 600
Inman, R. H., Pedro, H. T., and Coimbra, C. F.: Solar forecasting methods for renewable energy integration, Prog. Energ. Combust., 39, 535–576, 2013. 596
Iwabuchi, H.: Efficient Monte Carlo methods for radiative transfer modeling, J. Atmos. Sci., 63, 2324–2339, 2006. 595
Lee, W.-L., Liou, K., and Hall, A.: Parameterization of solar fluxes over mountain surfaces for application to climate models, J. Geophys. Res.-Atmos., 116, D01101, doi:10.1029/2010JD014722, 2011. 595
Liou, K.: An Introduction to Atmospheric Radiation, International Geophysics Series, vol. 84, 2nd. edn., Academic Press, San Diego, CA, 2002. 598
Long, C. N. and Ackerman, T. P.: Identification of clear skies from broadband pyranometer measurements and calculation of downwelling shortwave cloud effects, J. Geophys. Res., 105, 15609–15615. 2000. 608
MACC: available at: http://www.gmes-atmosphere.eu/ (last access: 7 November), 2013. 598
Manners, J., Vosper, S., and Roberts, N.: Radiative transfer over resolved topographic features for high-resolution weather prediction, Q. J. Roy. Meteor. Soc., 138, 720–733, 2012. 595
Mayer, B., Hoch, S. W., and Whiteman, C. D.: Validating the MYSTIC three-dimensional radiative transfer model with observations from the complex topography of Arizona's Meteor Crater, Atmos. Chem. Phys., 10, 8685–8696, doi:10.5194/acp-10-8685-2010, 2010. 595
Ohmura, A., Dutton, E. D., Forgan, B., Fröhlich, C., Gilgen, H., Hegner, H., Heimo, A., König-Langlo, G., McArthur, B., Müller, G., Philipona, R., Pinker, R., Whitlock, C., Dehne, K., and Wild, M.: Baseline Surface Radiation Network (BSRN/WCRP): new precision radiometry for climate research, B. Am. Meteorol. Soc., 79, 2115–2136, 1998. 605
Oreopoulos, L. and Barker, H. W.: Accounting for subgrid-scale cloud variability in a multi-layer 1d solar radiative transfer algorithm, Q. J. Roy. Meteor. Soc., 125, 301–330, 1999. 600
Pincus, R. and Evans, K. F.: Computational cost and accuracy in calculating three-dimensional radiative transfer: results for new implementations of Monte Carlo and SHDOM, J. Atmos. Sci., 66, 3131–3146, 2009. 595
Remer, L. A., Kaufman, Y., Tanré, D., Mattoo, S., Chu, D., Martins, J., Li, R.-R., Ichoku, C., Levy, R., Kleidman, R., Eck, T. F., Vermote, E., and Holben, B. N.: The MODIS aerosol algorithm, products, and validation, J. Atmos. Sci., 62, 947–973, 2005. 598

GMDD
7, 593–629, 2014

Ritter, B. and Geleyn, J.-F.: A comprehensive radiation scheme for numerical weather prediction models with potential applications in climate simulations, Mon. Weather Rev., 120, 303–325, 1992. 597

Ruiz-Arias, J. A., Cebecauer, T., Tovar-Pescador, J., and Šúri, M.: Spatial disaggregation of satellite-derived irradiance using a high-resolution digital elevation model, Sol. Energy, 84, 1644–1657, 2010. 595

Ruiz-Arias, J. A., Pozo-Váquez, D., Lara-Fanego, V., Santos-Alamillos, F. J., and Tovar-Pescador, J.: A high-resolution topographic correction method for clear-sky solar irradiance derived with a numerical weather prediction model, J. Appl. Meteorol. Clim., 50, 2460–2472, 2011. 595

Ruiz-Arias, J. A., Dudhia, J., Gueymard, C. A., and Pozo-Vázquez, D.: Assessment of the Level-3 MODIS daily aerosol optical depth in the context of surface solar radiation and numerical weather modeling, Atmos. Chem. Phys., 13, 675–692, doi:10.5194/acp-13-675-2013, 2013a. 597

Ruiz-Arias, J. A., Dudhia, J., Lara-Fanego, V., and Pozo-Vázquez, D.: A geostatistical approach for producing daily Level-3 MODIS aerosol optical depth analyses, Atmos. Environ., 79, 395–405, 2013b. 599

Ruiz-Arias, J. A., Dudhia, J., Santos-Alamillos, F. J., and Pozo-Vázquez, D.: Surface clear-sky shortwave radiative closure intercomparisons in the Weather Research and Forecasting model, J. Geophys. Res.-Atmos., 118, 9901–9913, 2013c. 596, 597, 599, 604, 605, 606, 607, 609

Shettle, E. P. and Fenn, R. W.: Models for the aerosols of the lower atmosphere and the effects of humidity variations on their optical properties, Tech. Rep. AFGL-TR-79-0214, Air Force Geophys. Lab., 1979. 600, 601, 603, 604, 626

GMDD
7, 593–629, 2014

Table 1. Spectral distribution in RRTMG. λ's in nm.

Band #	1	2	3	4	5	6	7	8	9	10	11	12	13	14
$\bar{\lambda}$	3462	2789	2325	2046	1784	1463	1271	1010.1	701.6	533.2	393.1	304.0	231.6	8021
λ_{min}	3077	2500	2150	1942	1626	1299	1242	778.2	625.0	441.5	344.8	263.2	200.0	3846
λ_{max}	3846	3077	2500	2150	1942	1626	1299	1242.0	778.2	625.0	441.5	344.8	263.2	12 195

GMDD
7, 593–629, 2014

Table 2. Ångström exponents for each band, aerosol type and relative humidity.

Relative humidity	α_i	0 %	50 %	70 %	80 %	90 %	95 %	98 %	99 %
Rural	α_1	1.036	1.035	1.030	0.999	0.946	0.906	0.818	0.753
	α_2	1.433	1.430	1.421	1.382	1.371	1.357	1.221	1.152
Urban	α_1	0.915	0.919	0.929	0.921	0.875	0.803	0.682	0.588
	α_2	1.198	1.202	1.202	1.254	1.265	1.243	1.164	1.082

GMDD
7, 593–629, 2014

Table A1. ρ_{rj} spectral scale LUT for rural aerosol.

RH	Band 1	Band 2	Band 3	Band 4	Band 5	Band 6	Band 7	Band 8	Band 9	Band 10	Band 11	Band 12	Band 13	Band 14
0 %	0.0738	0.1001	0.1286	0.1534	0.1887	0.2518	0.3017	0.4556	0.7163	1.0433	1.4023	1.7683	2.4499	0.0585
50 %	0.0742	0.1006	0.1291	0.1540	0.1894	0.2525	0.3024	0.4563	0.7168	1.0433	1.4018	1.7673	2.4478	0.0588
70 %	0.0755	0.1021	0.1308	0.1558	0.1914	0.2547	0.3047	0.4585	0.7183	1.0431	1.3995	1.7625	2.4372	0.0599
80 %	0.0810	0.1087	0.1383	0.1640	0.2003	0.2644	0.3148	0.4682	0.7248	1.0415	1.3853	1.7326	2.3727	0.0647
90 %	0.0826	0.1106	0.1405	0.1663	0.2028	0.2672	0.3177	0.4710	0.7266	1.0376	1.3614	1.6826	2.2664	0.0661
95 %	0.0848	0.1131	0.1434	0.1694	0.2062	0.2709	0.3215	0.4746	0.7289	1.0348	1.3436	1.6459	2.1894	0.0680
98 %	0.1085	0.1407	0.1741	0.2024	0.2415	0.3086	0.3602	0.5106	0.7522	1.0310	1.3054	1.5680	2.0289	0.0890
99 %	0.1230	0.1571	0.1922	0.2215	0.2616	0.3298	0.3816	0.5300	0.7642	1.0275	1.2779	1.5128	1.9180	0.1020

GMDD
7, 593–629, 2014

Table A2. ρ_{rj} spectral scale LUT for urban aerosol.

RH	Band 1	Band 2	Band 3	Band 4	Band 5	Band 6	Band 7	Band 8	Band 9	Band 10	Band 11	Band 12	Band 13	Band 14
0 %	0.1131	0.1460	0.1800	0.2086	0.2480	0.3155	0.3672	0.5170	0.7562	1.0389	1.3476	1.6541	2.2065	0.0932
50 %	0.1123	0.1450	0.1789	0.2075	0.2469	0.3143	0.3659	0.5159	0.7555	1.0391	1.3494	1.6578	2.2141	0.0924
70 %	0.1123	0.1450	0.1789	0.2075	0.2469	0.3143	0.3659	0.5159	0.7555	1.0399	1.3538	1.6669	2.2333	0.0924
80 %	0.1022	0.1334	0.1661	0.1938	0.2324	0.2990	0.3504	0.5016	0.7465	1.0381	1.3503	1.6596	2.2179	0.0834
90 %	0.1002	0.1311	0.1635	0.1911	0.2294	0.2959	0.3472	0.4987	0.7446	1.0344	1.3300	1.6180	2.1314	0.0816
95 %	0.1043	0.1358	0.1687	0.1967	0.2354	0.3022	0.3536	0.5046	0.7484	1.0294	1.2990	1.5551	2.0027	0.0852
98 %	0.1203	0.1541	0.1889	0.2181	0.2580	0.3260	0.3778	0.5266	0.7621	1.0220	1.2485	1.4548	1.8037	0.0996
99 %	0.1397	0.1758	0.2124	0.2428	0.2838	0.3527	0.4046	0.5505	0.7767	1.0168	1.2108	1.3814	1.6629	0.1172

GMDD
7, 593–629, 2014

Table A3. Single-scattering albedo LUT for rural aerosol.

RH	Band 1	Band 2	Band 3	Band 4	Band 5	Band 6	Band 7	Band 8	Band 9	Band 10	Band 11	Band 12	Band 13	Band 14
0 %	0.8730	0.6695	0.8530	0.8601	0.8365	0.7949	0.8113	0.8810	0.9305	0.9436	0.9532	0.9395	0.8007	0.8634
50 %	0.8428	0.6395	0.8571	0.8645	0.8408	0.8007	0.8167	0.8845	0.9326	0.9454	0.9545	0.9416	0.8070	0.8589
70 %	0.8000	0.6025	0.8668	0.8740	0.8503	0.8140	0.8309	0.8943	0.9370	0.9489	0.9577	0.9451	0.8146	0.8548
80 %	0.7298	0.5666	0.9030	0.9049	0.8863	0.8591	0.8701	0.9178	0.9524	0.9612	0.9677	0.9576	0.8476	0.8578
90 %	0.7010	0.5606	0.9312	0.9288	0.9183	0.9031	0.9112	0.9439	0.9677	0.9733	0.9772	0.9699	0.8829	0.8590
95 %	0.6933	0.5620	0.9465	0.9393	0.9346	0.9290	0.9332	0.9549	0.9738	0.9782	0.9813	0.9750	0.8980	0.8594
98 %	0.6842	0.5843	0.9597	0.9488	0.9462	0.9470	0.9518	0.9679	0.9808	0.9839	0.9864	0.9794	0.9113	0.8648
99 %	0.6786	0.5897	0.9658	0.9522	0.9530	0.9610	0.9651	0.9757	0.9852	0.9871	0.9883	0.9835	0.9236	0.8618

GMDD
7, 593–629, 2014

Table A4. Single-scattering albedo LUT for urban aerosol.

RH	Band 1	Band 2	Band 3	Band 4	Band 5	Band 6	Band 7	Band 8	Band 9	Band 10	Band 11	Band 12	Band 13	Band 14
0 %	0.4063	0.3663	0.4093	0.4205	0.4487	0.4912	0.5184	0.5743	0.6233	0.6392	0.6442	0.6408	0.6105	0.4094
50 %	0.4113	0.3654	0.4215	0.4330	0.4604	0.5022	0.5293	0.5848	0.6336	0.6493	0.6542	0.6507	0.6205	0.4196
70 %	0.4500	0.3781	0.4924	0.5050	0.5265	0.5713	0.6048	0.6274	0.6912	0.7714	0.7308	0.7027	0.6772	0.4820
80 %	0.5075	0.4139	0.5994	0.6127	0.6350	0.6669	0.6888	0.7333	0.7704	0.7809	0.7821	0.7762	0.7454	0.5709
90 %	0.5596	0.4570	0.7009	0.7118	0.7317	0.7583	0.7757	0.8093	0.8361	0.8422	0.8406	0.8337	0.8036	0.6525
95 %	0.6008	0.4971	0.7845	0.7906	0.8075	0.8290	0.8418	0.8649	0.8824	0.8849	0.8815	0.8739	0.8455	0.7179
98 %	0.6401	0.5407	0.8681	0.8664	0.8796	0.8968	0.9043	0.9159	0.9244	0.9234	0.9182	0.9105	0.8849	0.7796
99 %	0.6567	0.5618	0.9073	0.9077	0.9182	0.9279	0.9325	0.9398	0.9440	0.9413	0.9355	0.9278	0.9039	0.8040

GMDD
7, 593–629, 2014

Table A5. Asymmetry parameter LUT for rural aerosol.

RH	Band 1	Band 2	Band 3	Band 4	Band 5	Band 6	Band 7	Band 8	Band 9	Band 10	Band 11	Band 12	Band 13	Band 14
0 %	0.7444	0.7711	0.7306	0.7103	0.6693	0.6267	0.6169	0.6207	0.6341	0.6497	0.6630	0.6748	0.7208	0.7419
50 %	0.7444	0.7747	0.7314	0.7110	0.6711	0.6301	0.6210	0.6251	0.6392	0.6551	0.6680	0.6799	0.7244	0.7436
70 %	0.7438	0.7845	0.7341	0.7137	0.6760	0.6381	0.6298	0.6350	0.6497	0.6657	0.6790	0.6896	0.7300	0.7477
80 %	0.7336	0.7934	0.7425	0.7217	0.6925	0.6665	0.6616	0.6693	0.6857	0.7016	0.7139	0.7218	0.7495	0.7574
90 %	0.7111	0.7865	0.7384	0.7198	0.6995	0.6864	0.6864	0.6987	0.7176	0.7326	0.7427	0.7489	0.7644	0.7547
95 %	0.7009	0.7828	0.7366	0.7196	0.7034	0.6958	0.6979	0.7118	0.7310	0.7452	0.7542	0.7593	0.7692	0.7522
98 %	0.7226	0.8127	0.7621	0.7434	0.7271	0.7231	0.7248	0.7351	0.7506	0.7622	0.7688	0.7719	0.7756	0.7706
99 %	0.7296	0.8219	0.7651	0.7513	0.7404	0.7369	0.7386	0.7485	0.7626	0.7724	0.7771	0.7789	0.7790	0.7760

GMDD
7, 593–629, 2014

Table A6. Asymmetry parameter LUT for urban aerosol.

RH	Band 1	Band 2	Band 3	Band 4	Band 5	Band 6	Band 7	Band 8	Band 9	Band 10	Band 11	Band 12	Band 13	Band 14
0 %	0.7399	0.7372	0.7110	0.6916	0.6582	0.6230	0.6147	0.6214	0.6412	0.6655	0.6910	0.7124	0.7538	0.7395
50 %	0.7400	0.7419	0.7146	0.6952	0.6626	0.6287	0.6209	0.6280	0.6481	0.6723	0.6974	0.7180	0.7575	0.7432
70 %	0.7363	0.7614	0.7303	0.7100	0.6815	0.6550	0.6498	0.6590	0.6802	0.7032	0.7255	0.7430	0.7735	0.7580
80 %	0.7180	0.7701	0.7358	0.7163	0.6952	0.6807	0.6801	0.6935	0.7160	0.7370	0.7553	0.7681	0.7862	0.7623
90 %	0.7013	0.7733	0.7374	0.7203	0.7057	0.7006	0.7035	0.7192	0.7415	0.7596	0.7739	0.7827	0.7906	0.7596
95 %	0.6922	0.7773	0.7404	0.7264	0.7170	0.7179	0.7228	0.7389	0.7595	0.7746	0.7851	0.7909	0.7918	0.7562
98 %	0.6928	0.7875	0.7491	0.7393	0.7345	0.7397	0.7455	0.7602	0.7773	0.7883	0.7944	0.7970	0.7912	0.7555
99 %	0.7021	0.7989	0.7590	0.7512	0.7613	0.7746	0.7718	0.7727	0.7867	0.7953	0.7988	0.7994	0.7906	0.7600

GMDD
7, 593–629, 2014

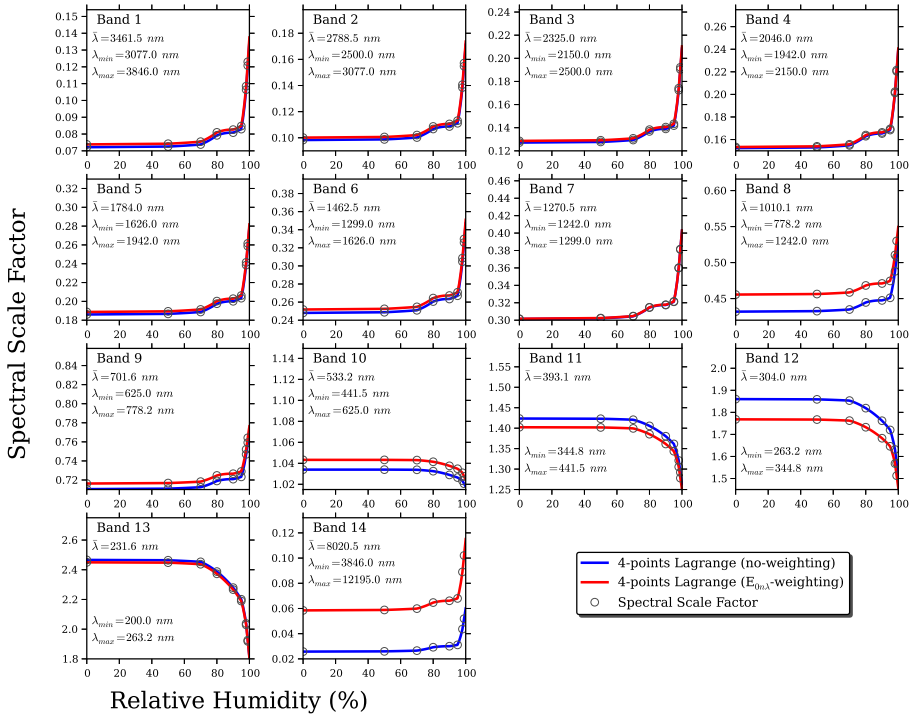

Fig. 1. AOD spectral scale factor interpolated using 4-point Lagrange interpolation for relative humidities from 0 % to 99 % for each RRTMG spectral band and the rural aerosol type. For the sake of comparison, the results using weighted and un-weighted spectral scale factors are shown.

GMDD
7, 593–629, 2014

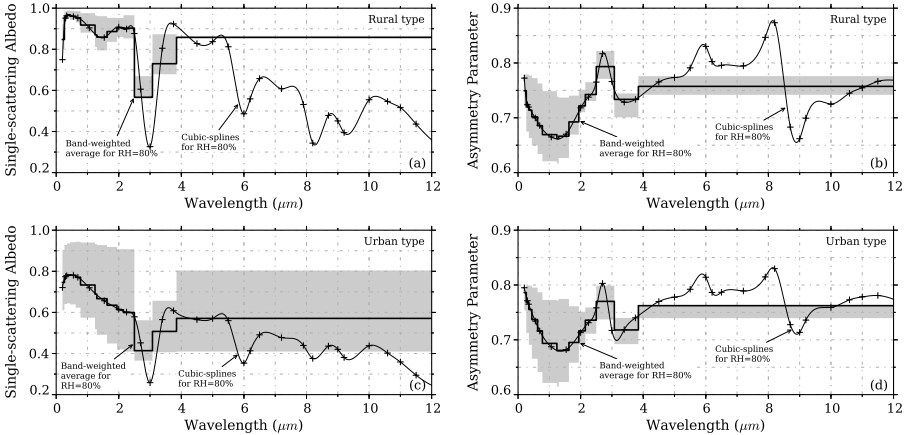

Fig. 2. Parameterized SSA and ASY parameters for the rural and urban aerosol types for a relative humidity of 80 % (thick line). The Shettle and Fenn (1979) spectral values are shown with cross marks. They have been interpolated using cubic splines (thin line). The grey region encompass the variability range of the parameters with different values of relative humidity.

GMDD
7, 593–629, 2014

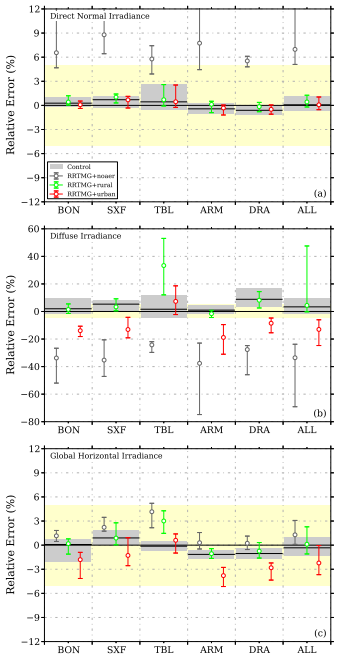

Fig. 3. Relative error of both the control experiment and the test cases as compared against the GHI, DNI and DIF ground observations at each site and the composite of all sites. The statistics are based on 767 samples for GHI and DIF and 892 for DNI. The number of samples per site varies between 150 and 200. The yellow-shaded area highlights the ±5 % error region as a rough reference of the expected observational error. The grey blocks refer to the control experiment and encompass the region around the mean relative error (horizontal black line) that contains 66 % of the experimental points at each site (33 % above the mean error, and 33 % below). The relative error obtained in the test cases is indicated with the vertical bars at each site. They also encompass 66 % of the experimental points, being the white circle mark the mean relative error.

GMDD
7, 593–629, 2014

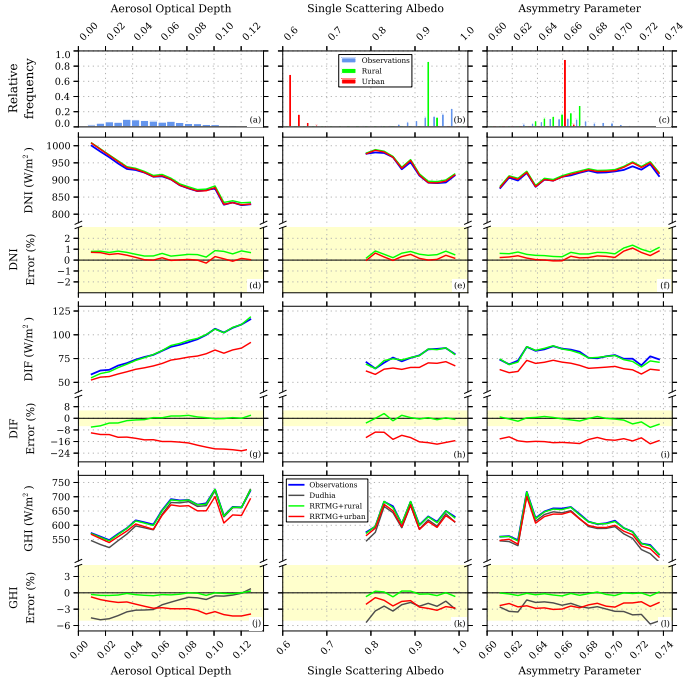

Fig. 4. Error analysis with respect to the variability range of AOD, SSA and ASY parameters for GHI, DNI and DIF resultant from the one-year WRF simulation. **(a–c)** shows the relative frequency distribution of the observed AOD at 0.55 µm, the observed and parameterized SSA values, and the observed and parameterized ASY values, respectively. **(d–l)** shows the observed and simulated DNI, DIF and GHI values (upper half of the panels) as well as their relative errors (lower half of the panels) as a function of the observed AOD at 0.55 µm, SSA and ASY values. The expected observational error region for the surface solar irradiance observations, roughly estimated as ±5 %, is highlighted in yellow.

GMDD
7, 593–629, 2014

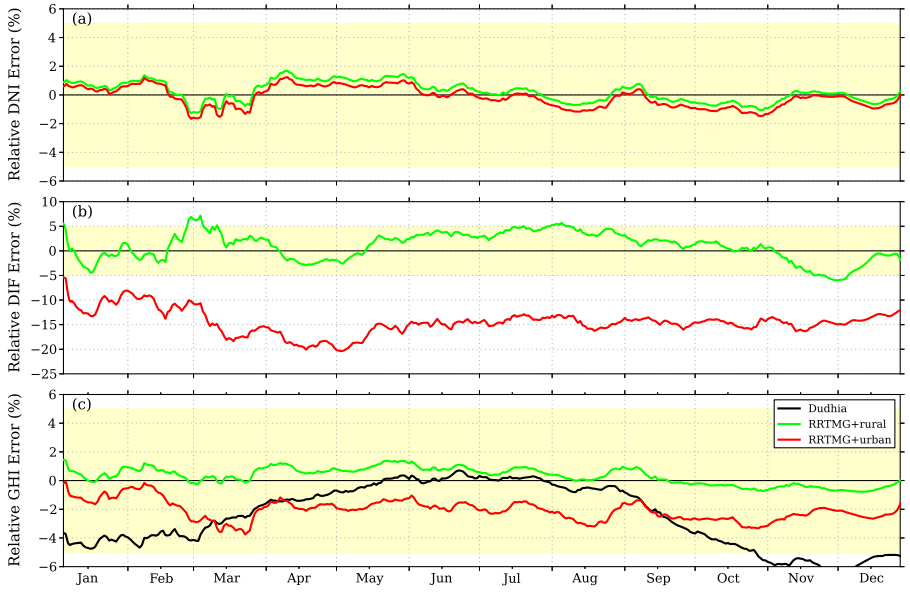

Fig. 5. Daily mean relative error in simulated DNI, DIF and GHI (simulated values minus observations) using the RRTMG model assuming rural and urban aerosol types, throughout the simulated year over the composite of the five experimental sites. A 15 day moving average filter has been used to make clear the bias trend. For GHI, the calculated values with the Dudhia scheme are also shown. The expected observational error region for the surface solar irradiance observations, roughly estimated as ±5 %, is highlighted in yellow.

GMDD
7, 593–629, 2014